Supplementary material

Methane Box Model

The effect of changes to global OH concentrations on global mean surface CH_4 concentrations is calculated in a simple global box model using the following equation:

$$\frac{1}{\Delta t}(X_{t+\Delta t} - X_t) = E - L = E - k[OH][X] \qquad (1)$$

where, X = global mean CH_4 in ppb, E = Annual emissions in Tg yr^{-1}, L = chemical loss to reaction with OH in Tg yr^{-1} and k = rate constant for reaction CH_4 + OH (k = 2.45×10^{-12} cm^3 $molecule^{-1}$ yr^{-1}) (Sander et al., 2011).

The model uses equation 1 to integrate global mean CH_4 based on annual mean emissions and chemical loss in time steps of 1 month. The relevant CH_4 emissions and monthly mean tropospheric OH concentrations from each simulations were used, with constant temperature (272.9 K).

Figure S1.

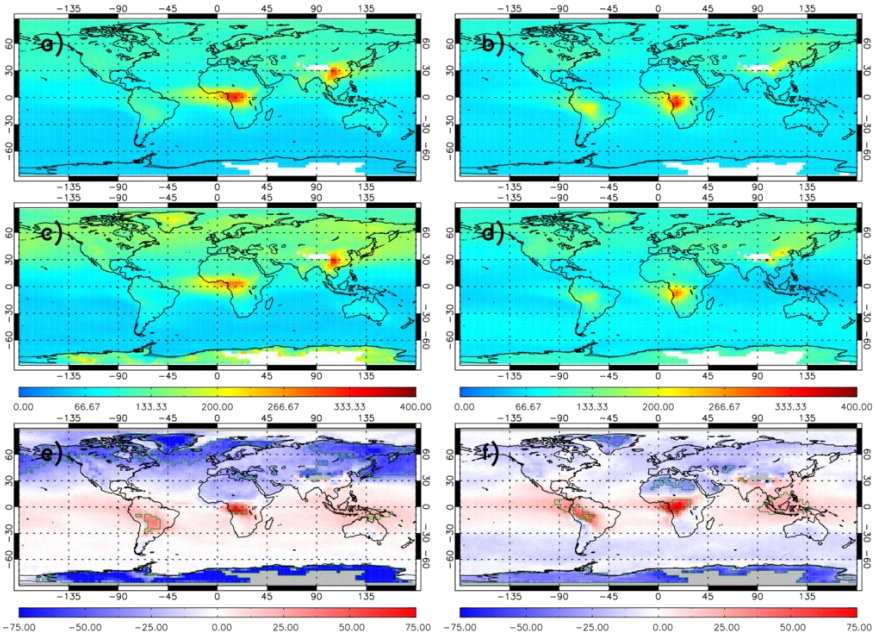

Figure S1: Carbon Monoxide (CO) at 800 hPa seasonal averages for 2007-2008. a) TOMCAT (December-January-February, DJF), b) TOMCAT (June-July-August, JJA), c) MOPITT DJF, d) MOPITT JJA, e) TOMCAT – MOPITT mean bias DJF and f) TOMCAT – MOPITT mean bias JJA. Green polygon-outlined regions show where the absolution model-satellite mean bias is greater than the satellite uncertainty (Emmons et al., 2004; Monks et al., 2017).

Figure S2.

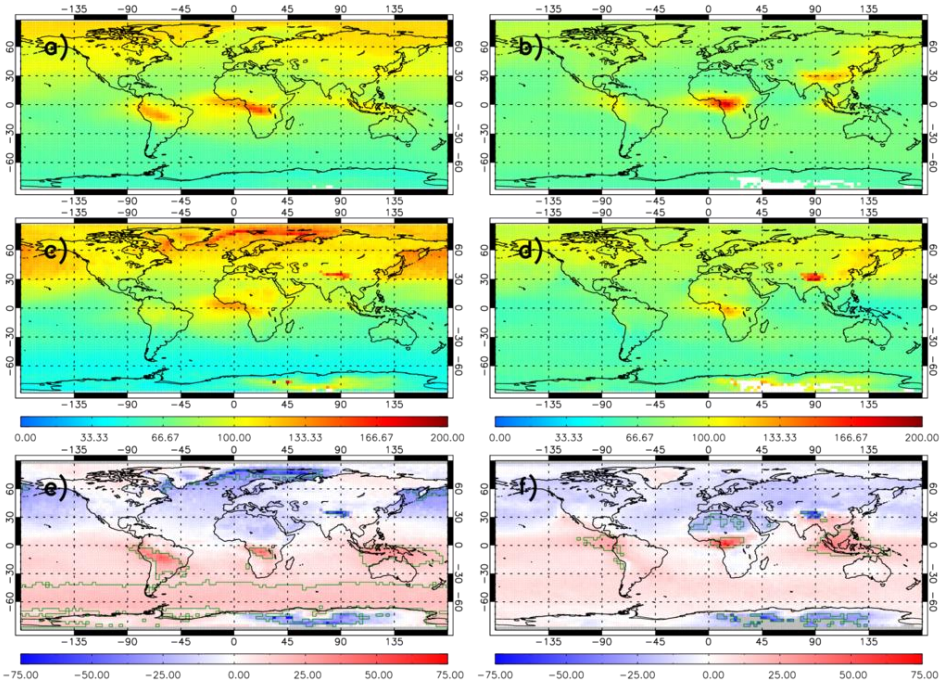

Figure S2: Carbon Monoxide (CO) at 500 hPa seasonal averages for 2007-2008. a) TOMCAT (December-January-February, DJF), b) TOMCAT (June-July-August, JJA), c) MOPITT DJF, d) MOPITT JJA, e) TOMCAT – MOPITT mean bias DJF and f) TOMCAT – MOPITT mean bias JJA. Green polygon-outlined regions show where the absolution model-satellite mean bias is greater than the satellite uncertainty (Emmons et al., 2004; Monks et al., 2017).

Figure S3.

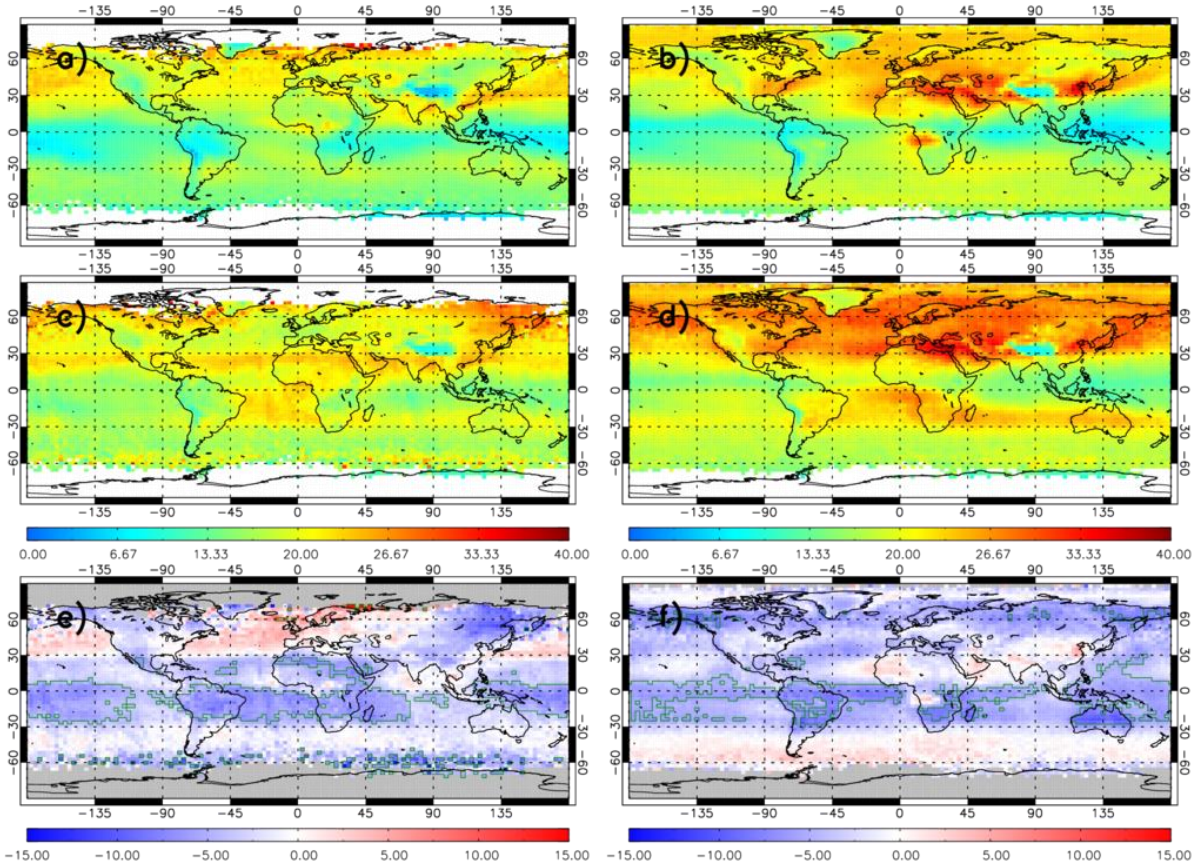

Figure S3: Sub-column (0-6 km) Ozone (O3) seasonal averages for 2007-2008 in Dobson units (DU). a) TOMCAT (December-January-February, DJF), b) TOMCAT (June-July-August, JJA), c) OMI DJF, d) OMI JJA, e) TOMCAT – OMI mean bias DJF and f) TOMCAT – OMI mean bias JJA. Green polygon-outlined regions show where the absolution model-satellite mean bias is greater than the satellite uncertainty (Miles et al., 2015).

Figure S4.

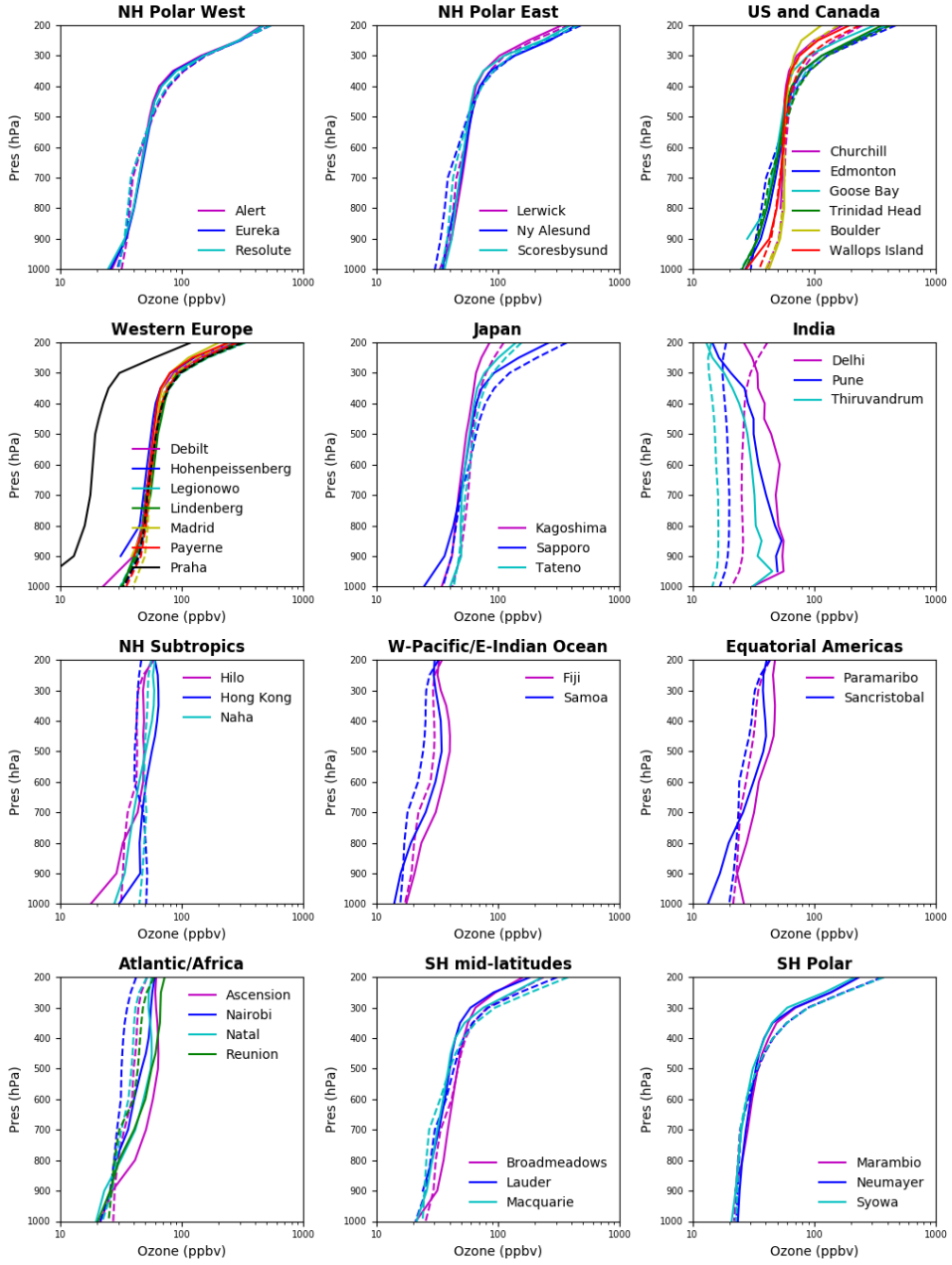

Figure S4: Annual mean ozone profiles from 1997-2011 simulated in TOMCAT (solid lines) evaluated against ozone sondes observations (dashed lines) from Tilmes (2011) climatology, 1995-2011.

Table S1 Aircraft campaign information from Emmons et al., (2010) climatologies.

Campaign	Date collected	Species	Location
TRACE-A	Sep 21 – Oct 26, 1992	O3, CO, NOx	East Brazil Coast (-35- -25N, 310-320E) East Brazil (-15- -5N, 310-320E) South Africa (-25- -5N, 15- 35E) South Atlantic (-20-0N, 340-350E) West Africa Coast (-25- -5N, 0-10E)
PEM-West-B	Feb 7 – Mar 14, 1994	CO, NOx	China Coast (20-30N, 115-130E) Japan (25-40N, 135-150E) Philippine Sea (5-20N, 135-150E)
TOTE	Dec 6 – 22, 1995	O3, CO, CH4	Alaska (60-70N, 205-220E) Hawaii (15-25N, 195-210N)
VOTE	Jan 20 – Feb 19, 1996	O3, CO, CH4	Alaska (60-70N, 205-220E) Hawaii (15-25N, 195-210N)
SUCCESS	Apr 15 – May 15, 1996	O3, CO	Central USA (35-40N, 260-265E)
PEM-Tropics-A	Aug 15-Oct 15, 1996	O3, CO, CH4, NOx	Christmas Island (0-10N, 200-220E) Easter Island (−40- −20N, 240-260E) Hawaii (10-30N, 190- 210E) Tahiti (−20- 0N, 200-230E)
POLINAT-2	Sep 19 – Oct 25, 1997	O3, CO, NOx	Canary Islands (25-35N, 340-350E) Eastern Atlantic (35-45N, 330-340E) Europe (45-55N, 5-15E) Ireland (50-60N, 345-355E)
SONEX	Oct 7 – Nov 12, 1997	O3, CO	East Atlantic (35-45N, 325-345E) Ireland (50-60N, 345-355E) Newfoundland (45-55N, 290-310E)
PEM-Tropics-B	Mar 6 – Apr 18, 1999	O3, CO, CH4, NOx	Christmas Island (0-10N, 200-220E) Easter Island (−40- −20N, 240-260E) Fiji (-30- -10N, 170-190E) Hawaii (10-30N, 190- 210E) Tahiti (−20- 0N, 200-230E
TOPSE	Feb 5 – May 23, 2000	O3, CH4, NOx	Boulder (37- 47N, 250-270E) Churchill (47-65N, 250-280E) Thule (65-90N, 250-300E)
TRACE-P	Feb 24 – Apr 10, 2001	O3, CO, CH4, NOx	China (10-30N, 110-130E) Guam (10-20N, 140-150E) Hawaii (10-30N, 190-210E) Japan (20-40N, 130-150E)

References

Emmons, L. K., Deeter, M. N., Gille, J. C., Edwards, D. P., Attié, J.-L., Warner, J., Ziskin, D., Francis, G., Khattatov, B., Yudin, V., Lamarque, J.-F., Ho, S.-P., Mao, D., Chen, J. S., Drummond, J., Novelli, P., Sachse, G., Coffey, M. T., Hannigan, J. W., Gerbig, C., Kawakami, S., Kondo, Y., Takegawa, N., Schlager, H., Baehr, J., and Ziereis, H.: Validation of Measurements of Pollution in the Troposphere (MOPITT) CO retrievals with aircraft in situ profiles, Journal of Geophysical Research: Atmospheres, 109, doi:10.1029/2003JD004101, 2004.

Miles, G. M., Siddans, R., Kerridge, B. J., Latter, B. G., and Richards, N. A. D.: Tropospheric ozone and ozone profiles retrieved from GOME-2 and their validation, Atmos. Meas. Tech., 8, 385-398, 10.5194/amt-8-385-2015, 2015.

Monks, S., R. Arnold, S., Hollaway, M., Pope, R., Wilson, C., Wuhu, F., Emmerson, K., J. Kerridge, B., Latter, B., M. Miles, G., Siddans, R., and P. Chipperfield, M.: The TOMCAT global chemical transport model v1.6: Description of chemical mechanism and model evaluation, 3025-3057 pp., 2017.

Sander, S. P., Abbatt, J., Barker, J., Burkholder, J. B., Friedl, R. R., Golden, D. M., Huie, R., Kurylo, M., Moortgat, G., Orkin, V., and Wine, P.: Chemical Kinetics and Photochemical Data for Use in Atmospheric Studies, Evaluation No. 17, 2011.